A theoretical analysis of billiard ball dynamics under cushion impacts

Article *in* ARCHIVE Proceedings of the Institution of Mechanical Engineers Part C Journal of Mechanical Engineering Science 1989-1996 (vols 203-210) · September 2010

DOI: 10.1243/09544062JMES1964

3 authors, including:

Senthan Mathavan
Nottingham Trent University
45 PUBLICATIONS **427** CITATIONS
SEE PROFILE

Robert Parkin
University of Bradford
180 PUBLICATIONS **1,562** CITATIONS
SEE PROFILE

A theoretical analysis of billiard ball dynamics under cushion impacts

S Mathavan*, **M R Jackson,** and **R M Parkin**
Mechatronics Research Group, Wolfson School of Mechanical and Manufacturing Engineering, Loughborough University, Loughborough, UK

The manuscript was received on 9 September 2009 and was accepted after revision for publication on 30 November 2009.

DOI: 10.1243/09544062JMES1964

Abstract: The last two decades have seen a growing interest in research related to billiards. There have been a number of projects aimed at developing training systems, robots, and computer simulations for billiards. Determination of billiard ball trajectories is important for all of these systems. The ball's collision with a cushion is often encountered in billiards and it drastically changes the ball trajectory, especially when the ball has spin. This work predicts ball bounce angles and bounce speeds for the ball's collision with a cushion, under the assumption of insignificant cushion deformation. Differential equations are derived for the ball dynamics during the impact and these equations are solved numerically. The numerical solutions together with previous experimental work by the authors predict that for the ball–cushion collision, the values of the coefficient of restitution and the sliding coefficient of friction are 0.98 and 0.14, respectively. A comparison of the numerical and experimental results indicates that the limiting normal velocity under which the rigid cushion assumption is valid is 2.5 m/s. A number of plots that show the rebound characteristics for given ball velocity–spin conditions are also provided. The plots quantify various phenomena that have hitherto only been described in the billiards literature.

Keywords: impulse with friction, billiards, snooker, pool, ball trajectories, cushion rebound, coefficient of restitution, impact simulations

1 INTRODUCTION

Snooker and pool are two popular cue sports generally known as billiards (here onwards the term 'billiards' is used to refer to both snooker and pool). Billiards is a classic example of dynamic concepts such as spinning, rolling, sliding, and the collisions of spheres. Billiards was one of the first games to be analysed from a technical perspective. The 1835 study by the French scientist Coriolis, entitled *Théorie mathématique des effets du jeu de billard*, is a pioneering work on sports dynamics [**1**]. Billiards-related research is steadily on the rise and in recent years a number of robots have been developed to play pool and snooker [**2**–**5**]. There are also a number of initiatives for creating training systems for billiard games [**6**–**8**]. The research on computer billiards, which simulates the real-world billiards environment, also receives the increasing attention of computer scientists seeking to create artificial intelligence that can formulate appropriate game-playing strategies [**9**–**11**].

Billiards is about manipulating the balls accurately on the table along different trajectories. This is performed so that all object balls are potted, in the given order, and the cue ball is left at an advantageous position on the table, after each shot, to play the next shot successfully. A player often uses cushion (or wall/rail/bumper) impacts to achieve planned trajectories. Cushion impacts give a great deal of variation to the game. The ball–cushion impacts change the ball trajectories dramatically when combined with the effects of ball spin and give the player a greater flexibility in his game strategy (see Fig. 1).

Previously, bounces of the ball off the cushion have been analysed by incorporating the coefficient of restitution between the ball and the cushion as the only influencing parameter and by considering the ball

*Corresponding author: *Department of Mechanical and Manufacturing Engineering, Loughborough University, Holywell Mechatronics Research Centre, Holywell Way, Loughborough, Leicestershire, LE11 3UZ, UK.*
email: S.Mathavan@lboro.ac.uk

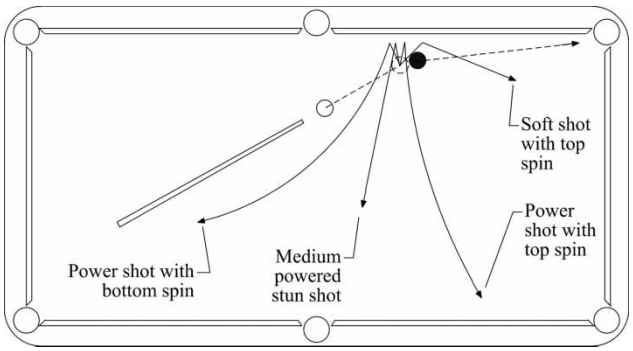

Fig. 1 Positioning the cue ball by its bounce off the cushion, by imparting different ball spins to it while still potting the object ball (shown in black)

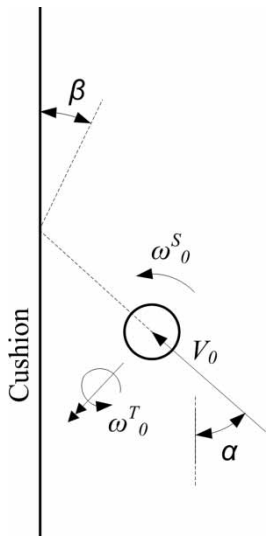

Fig. 2 Billiard ball prior to collision with a cushion

velocity normal to the cushion as the sole variable. According to current theory, and referring to Fig. 2, once the ball bounces off the cushion, it will have a velocity of $e_e V_0 \sin\alpha$ normal to the cushion, and a velocity $V_0 \cos\alpha$ along the cushion respectively, where e_e is the coefficient of restitution between the ball and the cushion. This simple analysis does not consider the effects of ball spin and the effect of friction during the impact, since it treats the collision as a purely two-dimensional (2D) phenomenon (the plane of analysis is as given in Fig. 2).

Ball spin, both sidespin ω_0^{S} and topspin ω_0^{T}, as shown in Fig. 2, are known to affect both the rebound speed and the rebound angle β of the ball. The latter two quantities are vital in order to estimate the trajectory of the ball after the cushion collision. Even though Marlow [**12**] tried to address these issues, the way the analysis was performed involved parameters like the impact time between the cushion and the ball for which the values were unknown. In addition, other assumptions made by Marlow, such as taking the direction of sliding between the ball and the cushion during the time of the impact as constant, do not seem correct (it is shown later that this keeps changing, throughout impact). Most importantly, Marlow's analysis is not complete.

This article presents a 3D analysis of the cushion–ball impact. For given input conditions (see Fig. 2), the analysis enables the calculation of the rebound conditions. This work will be useful for research on robotic billiards that involves trajectory calculations for the ball motion. Ball trajectory estimation is also necessary for the systems that are used to train amateur billiard players, as they need to instruct the player how a given shot (with a given velocity and spin) will change the configuration of the balls on the table. In addition, a computer simulation of billiards incorporating the knowledge from this 3D impact analysis would give the user a more realistic experience of the game. Furthermore, this work will also be of interest to the researchers working on the physics of billiards (for an exhaustive list of publications on billiard physics, see Alciatore [**13**]).

2 THEORY

The billiards cushion is made of pure gum rubber that has very good rebound properties. The cross-section of a typical billiard cushion is shown in Fig. 3. A slope is usually provided in the cushion such that its contact point on the ball is always above the horizontal great circle of the ball, in order to prevent the ball from leaping up in the air after impact. The following analysis assumes that the cushion does not change its geometry during the impact with the ball. This assumption may not be valid at high ball speeds, as the normal ball velocity at I (see Fig. 3), along the negative Z'-axis, will try to lift up the tip of the cushion. Also, the ball and the cushion are assumed to have a point contact, which again may not be true at larger ball speeds, as the ball will start to 'sink' more into the rubber cushion.

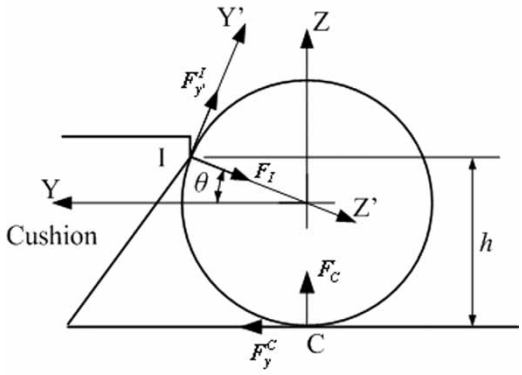

Fig. 3 Forces acting on the ball at the moment of collision: a side view along the cushion at table level

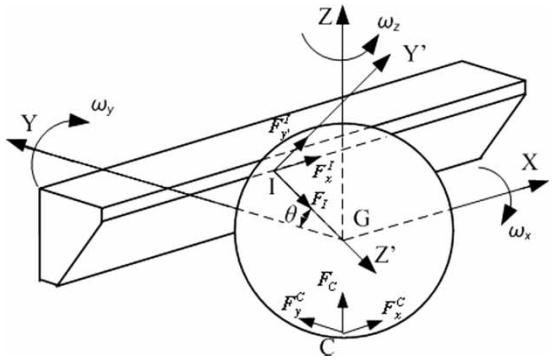

Fig. 4 Forces on the ball during impact (a part of the cushion is shown)

According to Fig. 3, the height of the contact point at the rail (i.e. I) is h. In both snooker and pool $h = 7R/5$, where R is the ball radius. The common normal line Z', at the contact point with the cushion, makes an angle of θ with the Y-axis, thus, $\sin\theta = 2/5$.

2.1 General equations of motion

Referring to Fig. 4, for the linear motion of the ball along the X-, Y-, and Z-directions, the following can be written

$$F_x^{\mathrm{I}} + F_x^{\mathrm{C}} = M\ddot{x}_{\mathrm{G}} \tag{1a}$$

$$-F_{\mathrm{I}}\cos\theta - F_{y'}^{\mathrm{I}}\sin\theta + F_y^{\mathrm{C}} = M\ddot{y}_{\mathrm{G}} \tag{1b}$$

$$-F_{\mathrm{I}}\sin\theta + F_{y'}^{\mathrm{I}}\cos\theta + F_{\mathrm{C}} - Mg = M\ddot{z}_{\mathrm{G}} \tag{1c}$$

Within the duration of the collision of the ball with the cushion, at any time instant $t = \tau$, consider an infinitesimally small time period $\Delta\tau$. Now, let ΔP denote the impulse or change in momentum due to the action of a general force F over $\Delta\tau$. Also, the accumulated total impact up to time T is denoted as P (and assuming that the impact started at $t = 0$); hence, it can be written that

$$\Delta P = \int_{\tau}^{\tau+\Delta\tau} F\,\mathrm{d}t \tag{2a}$$

and

$$P = \sum \Delta P = \int_0^{\mathrm{T}} F\,\mathrm{d}t \tag{2b}$$

The impulse–momentum relationship in conjunction with equation (2a), along the above directions results in the following equations

$$\Delta P_x^{\mathrm{I}} + \Delta P_x^{\mathrm{C}} = M\Delta\dot{x}_{\mathrm{G}} \tag{3a}$$

$$-\Delta P_{\mathrm{I}}\cos\theta - \Delta P_{y'}^{\mathrm{I}}\sin\theta + \Delta P_y^{\mathrm{C}} = M\Delta\dot{y}_{\mathrm{G}} \tag{3b}$$

$$-\Delta P_{\mathrm{I}}\sin\theta + \Delta P_{y'}^{\mathrm{I}}\cos\theta + \Delta P_{\mathrm{C}} = M\Delta\dot{z}_{\mathrm{G}} \tag{3c}$$

It should be noted that the impact component due to the force of gravity acting on the ball, mg, is absent in equation (3c). According to de la Torre Juárez [**14**], in the limit $\Delta t \to 0$, the non-diverging forces, such as the weight mg, will have a negligible contribution and thus will not influence the increase in momentum. It should also be noted that the slope shape of the cushion constrains the vertical motion of the ball. Hence, in equation (3c), $\Delta\dot{z}_{\mathrm{G}} = 0$. Equation (3c) is rearranged as

$$\Delta P_{\mathrm{C}} = \Delta P_{\mathrm{I}}\sin\theta - \Delta P_{y'}^{\mathrm{I}}\cos\theta \tag{3d}$$

Similarly, for the rotational motion of the ball about the X-axis, the following equation can be derived, with angular velocity being denoted by $\dot{\theta}$

$$(\Delta P_{y'}^{\mathrm{I}} + \Delta P_y^{\mathrm{C}})R = I\Delta\dot{\theta}_x$$

Where the moment of inertia of the ball $I = 2MR^2/5$, the above equation can be written as

$$\Delta P_{y'}^{\mathrm{I}} + \Delta P_y^{\mathrm{C}} = \frac{2MR}{5}\Delta\dot{\theta}_x \tag{4a}$$

Similarly, about the Y-axis and the Z-axis

$$\Delta P_x^{\mathrm{I}}\sin\theta - \Delta P_x^{\mathrm{C}} = \frac{2MR}{5}\Delta\dot{\theta}_y \tag{4b}$$

$$-\Delta P_x^{\mathrm{I}}\cos\theta = \frac{2MR}{5}\Delta\dot{\theta}_z \tag{4c}$$

2.2 Impact dynamics at I and C

At the contact point of the ball and the cushion, I, the ball will generally slip on the cushion (rolling can be treated as a special case of slipping, where the slipping velocity is zero). The slip will take place on the XY' plane (i.e. the tangential plane); also noting that the axis Y' is in the YZ plane. Let the slip speed of the ball at I be $s(t)$ at an angle $\Phi(t)$ with the X-axis. The instantaneous value of the normal impulse P_{I} according to equation (2b) will always be positive, since F_{I} is always positive. In addition, P_{I} monotonously increases with time t within the interval of impact. Therefore, P_{I} is considered as the independent variable for the analysis of impact instead of the regularly used variable of time t [**15**]. See Stronge [**15**] for an elaborative explanation of the other principles used within subsection 2.2.

Referring to Fig. 5, the slipping velocities along the X-axis and the Y'-axis are given by, respectively

$$\dot{x}_{\mathrm{I}} = s(P_{\mathrm{I}})\cos[\Phi(P_{\mathrm{I}})] \tag{5a}$$

$$\dot{y}'_{\mathrm{I}} = s(P_{\mathrm{I}})\sin[\Phi(P_{\mathrm{I}})] \tag{5b}$$

However, $\dot{y}'_{\mathrm{I}}$ can also be written as

$$\dot{y}'_{\mathrm{I}} = -\dot{y}_{\mathrm{I}}\sin\theta + \dot{z}_{\mathrm{I}}\cos\theta \tag{6}$$

Using the Amontons–Coulomb law of friction, for $s > 0$, also noting that the friction forces/impulses

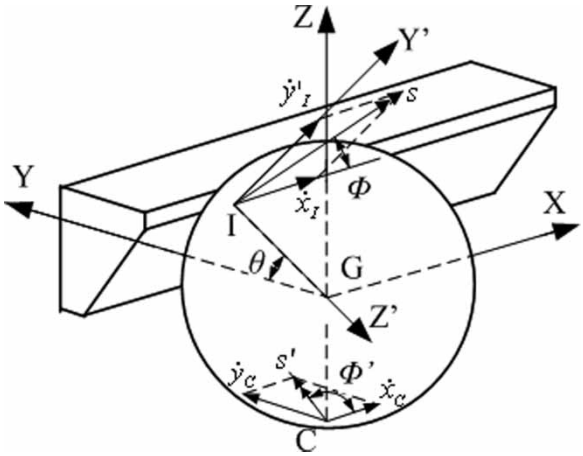

Fig. 5 Slip velocities at I and C

are opposite to the direction of sliding, the friction impulses along X and Y' are

$$\Delta P_x^{\mathrm{I}} = -\mu_{\mathrm{w}} \cos[\Phi(P_{\mathrm{I}})]\Delta P_{\mathrm{I}} \tag{7a}$$

$$\Delta P_{y'}^{\mathrm{I}} = -\mu_{\mathrm{w}} \sin[\Phi(P_{\mathrm{I}})]\Delta P_{\mathrm{I}} \tag{7b}$$

where μ_{w} is the coefficient of friction between the ball and the cushion.

From equations (3a) and (7b), the normal reaction from the table surface to the ball is given by

$$\Delta P_{\mathrm{C}} = \{\sin\theta + \mu_{\mathrm{w}} \sin[\Phi(P_{\mathrm{I}})] \cos\theta\}\Delta P_{\mathrm{I}} \tag{8}$$

Using the earlier argument, for the impact at C, the instantaneous impulse value P_{C} should be chosen as the independent variable. However, equation (8) shows that the value of P_{C} directly depends on the value of P_{I}. Hence, also for the impact at C, P_{I} is considered as the independent variable. This makes it possible to have P_{I} as the independent variable for all the impulse forces acting on the ball.

For the impact at C, the slip takes place within the XY plane. Let s' be the slip speed and Φ' be the direction of slip measured from the X-axis. Now, the components of s' along the X- and Y-directions are

$$\dot{x}_{\mathrm{C}} = s'(P_{\mathrm{I}}) \cos[\Phi'(P_{\mathrm{I}})] \tag{9a}$$

$$\dot{y}_{\mathrm{C}} = s'(P_{\mathrm{I}}) \sin[\Phi'(P_{\mathrm{I}})] \tag{9b}$$

Hereafter, the independent variable P_{I} is omitted from all equations for the sake of simplicity. When $s' > 0$, at C the impulse forces along the X and Y directions, also using equation (8), are

$$\begin{aligned}\Delta P_x^{\mathrm{C}} &= -\mu_{\mathrm{s}} \cos\Phi' \Delta P_{\mathrm{C}} \\ &= -\mu_{\mathrm{s}} \cos\Phi'(\sin\theta + \mu_{\mathrm{w}} \sin\Phi \cos\theta)\Delta P_{\mathrm{I}}\end{aligned} \tag{10a}$$

$$\begin{aligned}\Delta P_y^{\mathrm{C}} &= -\mu_{\mathrm{s}} \sin\Phi' \Delta P_{\mathrm{C}} \\ &= -\mu_{\mathrm{s}} \sin\Phi'(\sin\theta + \mu_{\mathrm{w}} \sin\Phi \cos\theta)\Delta P_{\mathrm{I}}\end{aligned} \tag{10b}$$

where μ_{s} is the coefficient of friction between the ball and the table surface.

2.3 Velocity relationships

The velocity of any point on the ball surface can be expressed in vector notation as

$$\boldsymbol{V} = \boldsymbol{V}_{\mathrm{G}} + \omega \boldsymbol{x} \boldsymbol{R}$$

where $\boldsymbol{V}$ is the vector that represents the linear velocity of a point on the ball surface, vector $\boldsymbol{V}_{\mathrm{G}}$ stands for the linear centroidal velocity of the ball, $\boldsymbol{\omega}$ is the vector denoting the rotational speed of the ball about its centroid, $\boldsymbol{R}$ is the vector defining the spatial location of such a surface point in relation to the ball centre, and $\boldsymbol{x}$ denotes the vector product, also known as the cross product.

Hence

$$\Delta \boldsymbol{V} = \Delta \boldsymbol{V}_{\mathrm{G}} + \Delta \boldsymbol{\omega} \boldsymbol{x} \boldsymbol{R} \tag{11}$$

From equation (11), resolving components along the axes appropriately, slip velocities along any axis can be expressed in terms of the centroid velocities of the ball.

At I

$$\Delta \dot{x}_{\mathrm{I}} = \Delta \dot{x}_{\mathrm{G}} + \Delta \dot{\theta}_y R \sin\theta - \Delta \dot{\theta}_z R \cos\theta \tag{12a}$$

$$\Delta \dot{y}'_{\mathrm{I}} = -\Delta \dot{y}_{\mathrm{G}} \sin\theta + \Delta \dot{z}_{\mathrm{G}} \cos\theta + \Delta \dot{\theta}_x R \tag{12b}$$

Similarly at C, along the X-axis

$$\Delta \dot{x}_{\mathrm{C}} = \Delta \dot{x}_{\mathrm{G}} - \Delta \dot{\theta}_y R \tag{13a}$$

and along the Y-axis

$$\Delta \dot{y}_{\mathrm{C}} = \Delta \dot{y}_{\mathrm{G}} + \Delta \dot{\theta}_x R \tag{13b}$$

Equations (12) and (13) make it possible to estimate the slip velocities and the slip angles of the ball, both at the table and at the cushion interface.

2.4 A description of ball dynamics

When substituting the expressions for ΔP_x^{I} and ΔP_x^{C} from equations (7a) and (10a) in equation (3a), $\Delta \dot{x}_{\mathrm{G}}$, which is the increment in the centroid velocity in the X direction $\dot{x}_{\mathrm{G}}$, is expressed in terms of the slip angles Φ and Φ' by

$$\begin{aligned}\Delta \dot{x}_{\mathrm{G}} = -\frac{1}{M}[&\mu_{\mathrm{w}} \cos\Phi + \mu_{\mathrm{s}} \cos\Phi' \\ &\times (\sin\theta + \mu_{\mathrm{w}} \sin\Phi \cos\theta)]\Delta P_{\mathrm{I}}\end{aligned}$$

As $\Delta P_{\mathrm{I}} \to 0$ this equation will become

$$\frac{\mathrm{d}\dot{x}_{\mathrm{G}}}{\mathrm{d}P_{\mathrm{I}}} = -\frac{1}{M}[\mu_{\mathrm{w}} \cos\Phi + \mu_{\mathrm{s}} \cos\Phi' \times (\sin\theta + \mu_{\mathrm{w}} \sin\Phi \cos\theta)] \tag{14a}$$

Similarly, it could be shown that

$$\frac{\mathrm{d}\dot{y}_{\mathrm{G}}}{\mathrm{d}P_{\mathrm{I}}} = -\frac{1}{M}[\cos\theta - \mu_{\mathrm{w}} \sin\theta \sin\Phi + \mu_{\mathrm{s}} \sin\Phi'(\sin\theta + \mu_{\mathrm{w}} \sin\Phi \cos\theta)] \tag{14b}$$

$$\frac{\mathrm{d}\dot{z}_{\mathrm{G}}}{\mathrm{d}P_{\mathrm{I}}} = 0 \tag{14c}$$

$$\frac{\mathrm{d}\dot{\theta}_x}{\mathrm{d}P_{\mathrm{I}}} = -\frac{5}{2MR}[\mu_{\mathrm{w}} \sin\Phi + \mu_{\mathrm{s}} \sin\Phi' \times (\sin\theta + \mu_{\mathrm{w}} \sin\Phi \cos\theta)] \tag{14d}$$

$$\frac{\mathrm{d}\dot{\theta}_y}{\mathrm{d}P_{\mathrm{I}}} = -\frac{5}{2MR}[\mu_{\mathrm{w}} \cos\Phi \sin\theta - \mu_{\mathrm{s}} \cos\Phi' \times (\sin\theta + \mu_{\mathrm{w}} \sin\Phi \cos\theta)] \tag{14e}$$

$$\frac{\mathrm{d}\dot{\theta}_z}{\mathrm{d}P_{\mathrm{I}}} = \frac{5}{2MR}(\mu_{\mathrm{w}} \cos\Phi \cos\theta) \tag{14f}$$

The differential equations in equation (14) describe the motion of the ball completely. The slip angles Φ and Φ' can be replaced by the centroidal velocities $\{\dot{x}_{\mathrm{G}}, \dot{y}_{\mathrm{G}}, \dot{z}_{\mathrm{G}}, \dot{\theta}_x, \dot{\theta}_y, \dot{\theta}_z\}$, by using the relationships derived in section 2.3, resulting in six simultaneous first-order, second-degree, differential equations in $\{\dot{x}_{\mathrm{G}}, \dot{y}_{\mathrm{G}}, \dot{z}_{\mathrm{G}}, \dot{\theta}_x, \dot{\theta}_y, \dot{\theta}_z\}$. An analytical solution for these differential equations is extremely difficult to find. However, a numerical solution is still possible, and the forms as given in equation (14) can be directly used in the numerical scheme.

3 NUMERICAL SOLUTION

As seen already, the solution to the set of six differential equations will involve a numerical method. The numerical algorithm has to be supplied with the initial conditions for the ball velocity, the conditions under which different motion transitions (such as sliding to rolling) take place, and numerical values for the parameters involved in the equations, such as μ_s.

3.1 Initial conditions

Referring to Fig. 2, the initial conditions for the centroid velocities of the ball are

$$(\dot{x}_{\mathrm{G}})_1 = V_0 \cos\alpha, \quad (\dot{y}_{\mathrm{G}})_1 = V_0 \sin\alpha, \quad (\dot{z}_{\mathrm{G}})_1 = 0,$$
$$(\dot{\theta}_x)_1 = -\omega_0^{\mathrm{T}} \sin\alpha, \quad (\dot{\theta}_y)_1 = \omega_0^{\mathrm{T}} \cos\alpha, \quad \text{and}$$
$$(\dot{\theta}_z)_1 = \omega_0^{\mathrm{S}}$$

the initial slip speeds at I and C are

$$s(0) = \left| \sqrt{\begin{matrix}[V_0 \cos\alpha + R(\omega_0^{\mathrm{T}} \cos\alpha \sin\theta - \omega_0^{\mathrm{S}} \cos\theta)]^2 \\ +[-V_0 \sin\alpha \sin\theta - R\omega_0^{\mathrm{T}} \sin\alpha]^2\end{matrix}} \right|$$
$$s'(0) = |V_0 - R\omega_0^{\mathrm{T}}|$$

and the slip angles are

$$\Phi(0) = \tan^{-1}\left[\frac{-V_0 \sin\alpha \sin\theta - R\omega_0^{\mathrm{T}} \sin\alpha}{V_0 \cos\alpha + R(\omega_0^{\mathrm{T}} \cos\alpha \sin\theta - \omega_0^{\mathrm{S}} \cos\theta)}\right]$$
$$\Phi'(0) = \begin{cases} \alpha & \text{for} \quad V_0 - R\omega_0^{\mathrm{T}} > 0 \\ 180^\circ + \alpha & \text{for} \quad V_0 - R\omega_0^{\mathrm{T}} < 0 \end{cases}$$

where α is the incident angle of the ball.

$\Phi'(0)$ is not defined for the condition $V_0 - R\omega_0^{\mathrm{T}} = 0$, as the ball rolls on the table under this condition.

3.2 Friction coefficients and conditions for rolling

During the rolling phase slip speed s (or s' for the sliding on the table-felt) becomes zero. In this instance, the relative motion between bodies stops at their contact point along the common tangent and the frictional forces become null (the effects of stick are neglected).

1. For the condition $s = 0$, the ball will be rolling on the cushion at I. $\Delta P_x^{\mathrm{I}} = \Delta P_{y'}^{\mathrm{I}} = 0$, and from equation (3c), $\Delta P_{\mathrm{C}} = 0$. Hence

$$\Delta P_x^{\mathrm{C}} = \Delta P_y^{\mathrm{C}} = 0 \tag{15a}$$

2. For the condition $s' = 0$, the ball will roll on the table surface, and

$$\Delta P_x^{\mathrm{C}} = \Delta P_y^{\mathrm{C}} = 0 \tag{15b}$$

High-speed-camera-based measurements were used, in a previous work by the present authors, to determine the sliding coefficient of friction between a snooker ball and the table-felt; the sliding coefficient of friction μ_{s} was found to be between 0.178 and 0.245 [**16**]. Marlow [**12**] suggests a value of 0.2 for the game of pool. Since the present authors have performed extensive measurements of the various parameters related to snooker [**16**], from here onwards the numerical values found in snooker are used for the calculations. μ_{s} is assumed to be 0.212, as an average value. For a snooker ball, $M = 0.1406$ kg and $R = 26.25$ mm.

3.3 Coefficient of restitution and impact mechanics

According to Stronge [**15**], the energetic coefficient of restitution e_{e} is independent of friction and the process of slip. e_{e}^2 is the negative of the ratio of the work done

by the impulse force during the restitution phase to that during the compression phase. The work done at I by the forces acting along the axis Z' is

$$\Delta W_{Z'_\mathrm{I}} = \int_{\tau}^{\tau+\Delta\tau} F_\mathrm{I}\dot{z}'_\mathrm{I}\,\mathrm{d}t = \int_{P_\mathrm{I}}^{P_\mathrm{I}+\Delta P_\mathrm{I}} \dot{z}'_\mathrm{I}\,\mathrm{d}P_\mathrm{I}$$

Its numerical form is

$$(W_{Z'_\mathrm{I}})_{n+1} - (W_{Z'_\mathrm{I}})_n = \Delta P_\mathrm{I}\frac{[(\dot{z}'_\mathrm{I})_{n+1} + (\dot{z}'_\mathrm{I})_n]}{2} \tag{16a}$$

where $\dot{z}'_\mathrm{I}$ is the relative velocity between the ball and the cushion in the direction of the common normal at I (here it is assumed that the cushion does not move sufficiently to affect a change in the relative velocity (i.e. the cushion is treated as a rigid body)). F_I is the normal force from the cushion acting on the ball. When P_I^f and P_I^c denote the accumulated impulse at the termination of impulse and at the termination of compression, respectively, it can be shown that [**15**]

$$e_\mathrm{e}^2 = \frac{-\int_{P_\mathrm{I}^\mathrm{c}}^{P_\mathrm{I}^\mathrm{f}} \dot{z}'_\mathrm{I}\,\mathrm{d}P_\mathrm{I}}{\int_0^{P_\mathrm{I}^\mathrm{c}} \dot{z}'_\mathrm{I}\,\mathrm{d}P_\mathrm{I}}$$

Rearranging the equation

$$W_{Z'_\mathrm{I}}(P_\mathrm{I}^\mathrm{f}) = (1 - e_\mathrm{e}^2)W_{Z'_\mathrm{I}}(P_\mathrm{I}^\mathrm{c}) \tag{16b}$$

The termination of compression occurs when the normal component of the relative velocity becomes zero, that is

$$\dot{z}'_\mathrm{I}(P_\mathrm{I}^\mathrm{c}) = 0 \tag{16c}$$

According to Marlow [**12**], the coefficient of restitution between the cushion and the ball, e_e, is 0.55 for pool. However, the authors of this work have obtained an experimental plot for the ball–cushion impact in snooker, where a snooker ball, under the conditions of rolling ($\omega_0^\mathrm{T} = V_0/R$) and no sidespin ($\omega_0^\mathrm{S} = 0$), was shot to collide with the cushion perpendicularly ($\alpha = 0$), and tracked using a machine vision camera [**15**]. The incident versus rebound speed plot obtained was used to conclude that the equivalent coefficient of restitution for a rolling ball perpendicularly colliding with the cushion has a value of 0.818, on average; the experimental procedure is briefly outlined in section 3.5. Here it must be noted that the value of 0.818 incorporates the effects of friction and the three-dimensionality of the impulse configuration, and only stands as a representative value for the coefficient of restitution.

3.4 Numerical algorithm

Equations (14) have equivalent algebraic forms as

$$(\dot{x}_\mathrm{G})_{n+1} - (\dot{x}_\mathrm{G})_n = -\frac{1}{M}\{\mu_\mathrm{w}\cos(\Phi)_n + \mu_\mathrm{s}\cos(\Phi')_n \times [\sin\theta + \mu_\mathrm{w}\sin(\Phi)_n\cos\theta]\}\Delta P_\mathrm{I} \tag{17a}$$

where, using equation sets (12) and (13)

$$\tan(\Phi)_n = \frac{-(\dot{y}_\mathrm{G})_n\sin\theta + (\dot{z}_\mathrm{G})_n\cos\theta + (\dot{\theta}_x)_n R}{(\dot{x}_\mathrm{G})_n + (\dot{\theta}_y)_n R\sin\theta - (\dot{\theta}_z)_n R\cos\theta}$$

and

$$\tan(\Phi')_n = \frac{(\dot{y}_\mathrm{G})_n + (\dot{\theta}_x)_n R}{(\dot{x}_\mathrm{G})_n - (\dot{\theta}_y)_n R}$$

A numerical scheme is written in MATLAB® programming language. The values of V_0, ω_0^T, ω_0^S, and α are the inputs to the scheme. The scheme calculates the changes in the values of V_0, ω_0^T, ω_0^S, and α by incrementing P_I in small step sizes. The smaller the value of the increment in impulse P_I (i.e. ΔP_I) in equation (15a), the more accurate the results. The aim is to find the centroid velocities of the balls at the final accumulated impulse value P_I^f.

The numerical scheme, as shown in Fig. 6, starts by calculating the initial centroidal velocities and the corresponding slip speeds and slip angles as illustrated in section 3.1. In addition, arrays to store the intermediate values of the centroidal velocities and slip speeds and slip angles for each increment in the form of ΔP_I are also initiated. Then the algorithm continues its operation by calculating increments in the centroid velocities of the ball by using equation (17a) and five other simultaneous equations. Using these increments and equations (12a), (12b), (13a), and (13b) the new slip velocities are calculated. The code is designed to incorporate the modifications necessary when a rolling condition is reached at either of the sliding contacts, as given in equations (15a) and (15b). The values of ball velocities are saved as arrays, including the work done at I along the Z'-axis (i.e. $W_{Z'_\mathrm{I}}$, calculated from equation (16a)). The latest parameter values are appended to these arrays once each ΔP_I is applied.

Again, P_I^f cannot be found analytically and has to be obtained numerically using equations (16a) and (16b). The numerical scheme is initially stopped when $\dot{z}'_\mathrm{I} = 0$ (i.e. when the compression phase has ended), and the corresponding value of work done is obtained from the array containing $W_{Z'_\mathrm{I}}$, which will be $W_{Z'_\mathrm{I}}(P_\mathrm{I}^\mathrm{c})$. Now, using equation (16b), the value $W_{Z'_\mathrm{I}}(P_\mathrm{I}^\mathrm{f})$ can be calculated, given that e_e is known. The numerical process of incrementing P_I can resume again, and when $W_{Z'_\mathrm{I}} = W_{Z'_\mathrm{I}}(P_\mathrm{I}^\mathrm{f})$, the process is terminated. The rebound velocity values of the ball centroid are the last entries in the arrays of the respective velocity components.

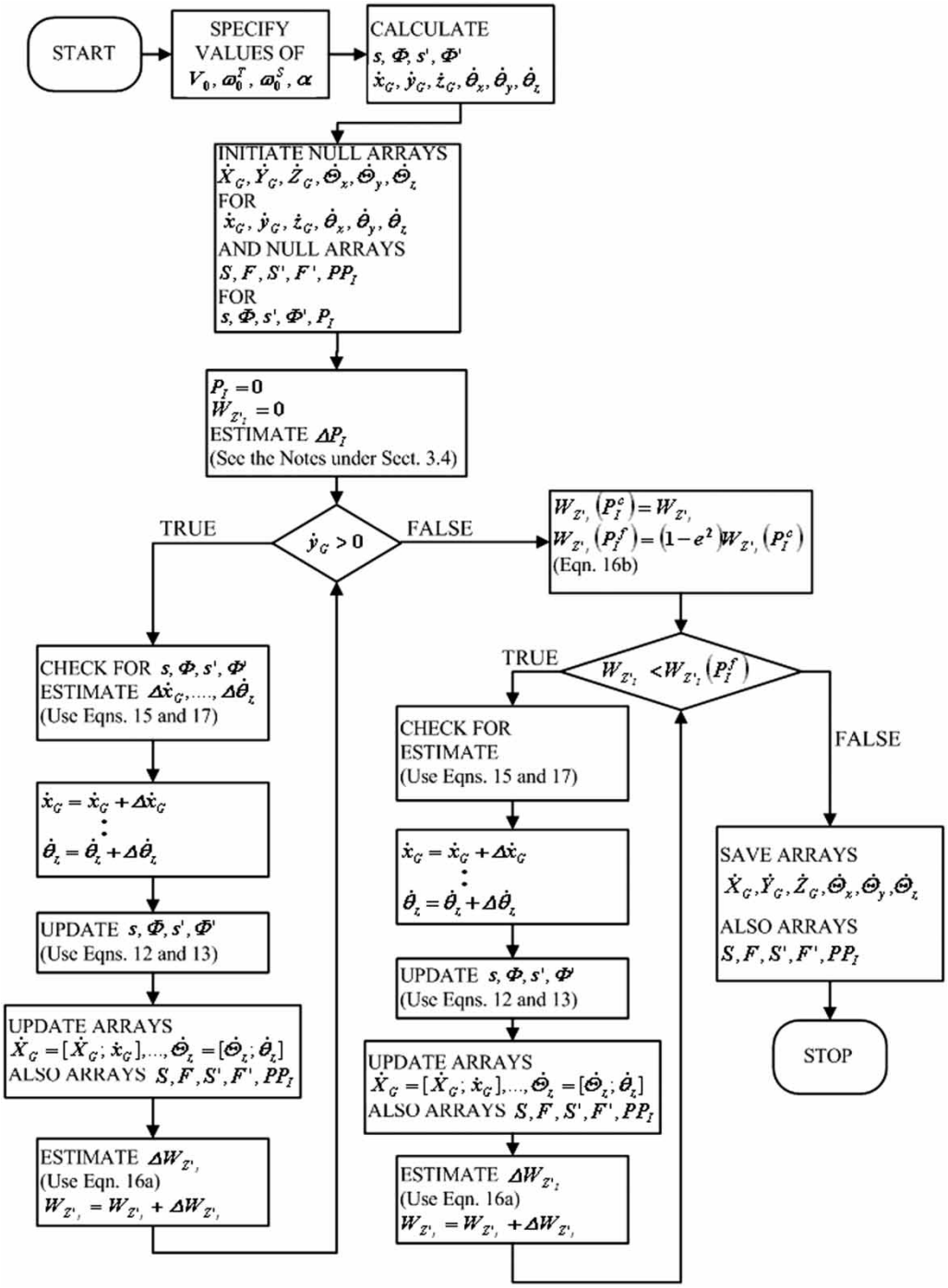

Fig. 6 Flowchart of the numerical algorithm

Note: in order to start the numerical scheme, a reasonable value for ΔP_{I} has to be assumed. An approximate value for $P_{\mathrm{I}}^{\mathrm{f}}$ can be assumed to be $(1+e_{\mathrm{e}})MV_0 \sin\alpha$, which is the value of the final accumulated normal impulse for a horizontally moving, non-spinning ball colliding into a solid vertical wall. Hence, approximately for N iterations, $\Delta P_I = [(1+e_{\mathrm{e}})MV_0 \sin\alpha/N]$. Obviously the values of $P_{\mathrm{I}}^{\mathrm{c}}$ and $P_{\mathrm{I}}^{\mathrm{f}}$ will decide the actual number of iterations that have taken place in the scheme. An initial N of 5000 worked satisfactorily for the scheme.

3.5 Estimating e_{e} and μ_{w}

The experimental plot in Fig. 7 was obtained under the conditions of $\omega_0^{\mathrm{S}} = 0$, $\alpha = 90^\circ$, and $\omega_0^{\mathrm{T}} = V_0/R$, on a Riley® Renaissance-type snooker table, which is also the official table brand of the World Snooker Association and is used in all its professional tournaments. The ball speed is calculated from an experimental procedure involving a stationary high-speed camera (the general experimental procedure is explained in Mathavan *et al.* [**16**]). It is known that $0 < e_{\mathrm{e}} \leqslant 1$. For

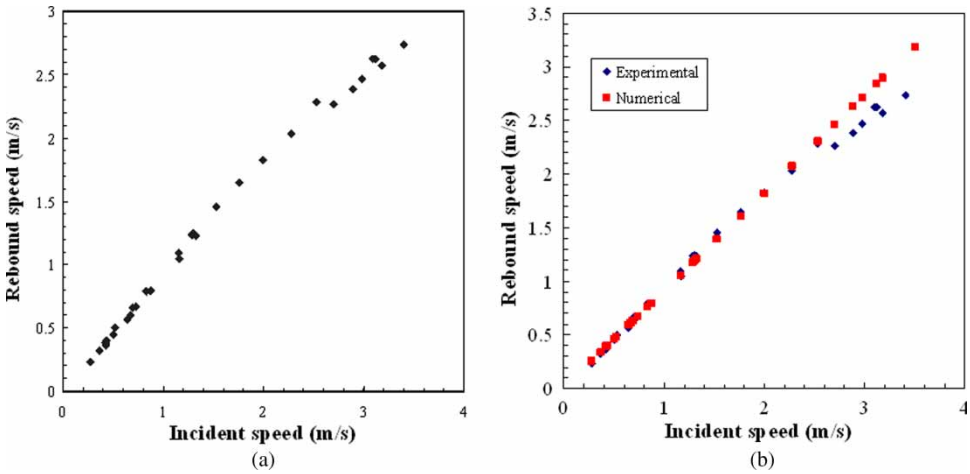

Fig. 7 Rebound speed versus incident velocity, obtained experimentally and numerically

each of the experimentally obtained incident speed values (i.e. V_0) in the speed range $V_0 < 1.5$ m/s, the numerical algorithm was run for values of e_e and μ_w between 0 and 1 in increments of 0.01, and the rebound speed $\dot{y}_G(P_I^f)$ was obtained. Higher incident speeds were not considered, as the assumption of a rigid cushion may not then be applicable. The values of e_e and μ_w that minimize the root mean square (RMS) value of the error between the experimental and the numerically predicted rebound speeds should be the actual value for the coefficient of restitution between the cushion and the ball. Calculations showed that the RMS error was a minimum when $e_e = 0.98$ and $\mu_w = 0.14$.

Numerically obtained rebound speed values for $e_e = 0.98$ and $\mu_w = 0.14$ are plotted in Fig. 7 together with the experimentally obtained values. As seen in Fig. 7(b), numerically obtained values of the incident speed deviate from the experimentally obtained values for speeds $V_0 > 2.5$ m/s. $V_0 > 2.5$ m/s is, quite possibly, the velocity limit under which the rigid body assumption for the cushion would be valid. $V_0 = 2.5$ m/s is a considerably high ball speed as far as snooker is concerned. For oblique shots, only the ones for which the normal component of the incident velocity of less than 2.5 m/s would be analysed using the numerical algorithm described in section 3.4.

4 RESULTS AND DISCUSSION

The results obtained from the numerical algorithm for various speed–spin combinations are given in Figs 8 to 10.

In billiards, once the ball is struck by the cue stick, the ball generally slides, where $\omega_0^T \neq V_0/R$. However,

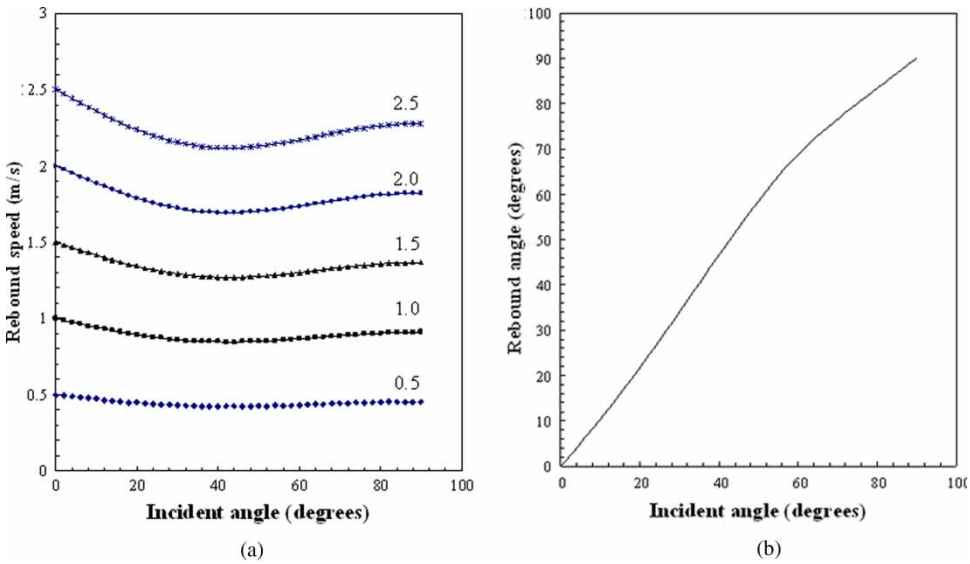

Fig. 8 Rebound speed and rebound angle versus incident angle for different rolling velocities with no sidespin ($\omega_0^T = V_0/R$, $\omega_0^S = 0$)

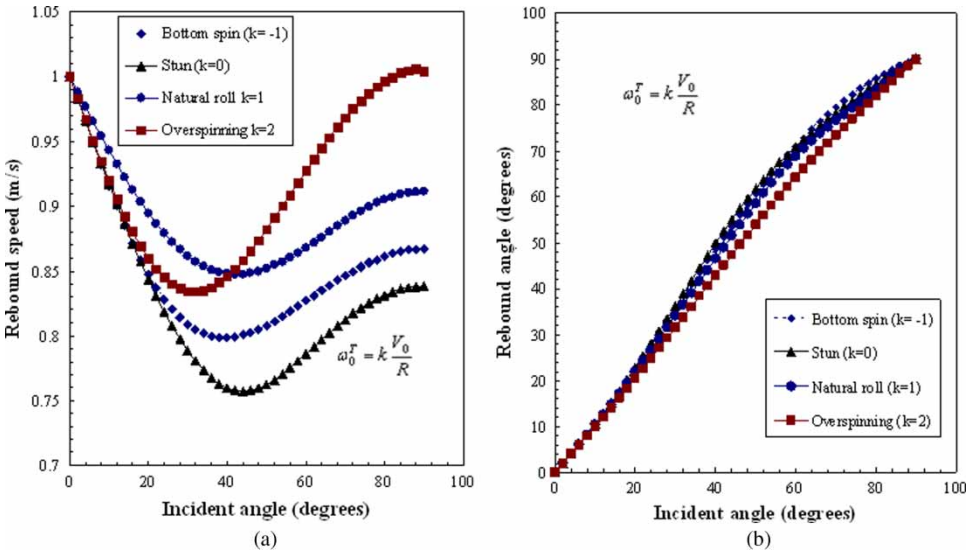

Fig. 9 Rebound speed and rebound angle versus incident angle for different topspins of the ball, $\omega_0^{\mathrm{T}} = kV_0/R$ and $V_0 = 1$ m/s with no sidespin ($\omega_0^{\mathrm{S}} = 0$)

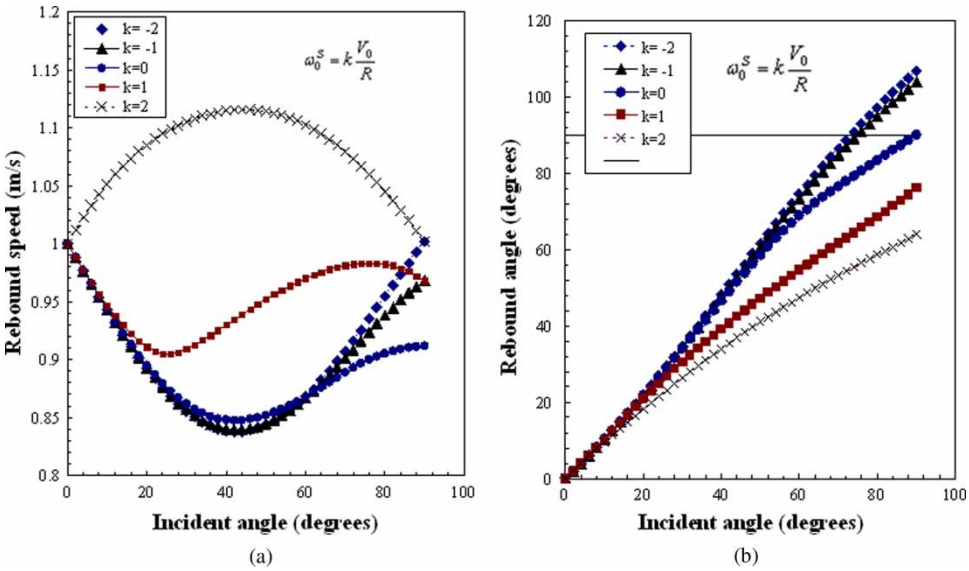

Fig. 10 Rebound speed and rebound angle versus incident angle for different sidespins of the ball, $\omega_0^{\mathrm{S}} = kV_0/R$ and $V_0 = 1$ m/s with the ball rolling ($\omega_0^{\mathrm{T}} = V_0/R$)

the rolling condition of $\omega_0^{\mathrm{T}} = V_0/R$ is quickly achieved by the action of friction between the ball and the table (an interested reader can refer to the camera-based tracking plots given in reference [**16**]). Hence, in most instances, the ball is likely to be in rolling mode when it collides with a cushion, also possibly with some sidespin. The plots for the simplest case of rolling with no sidespin are shown in Fig. 8. The plot of rebound speed versus incident angle for different incident ball speeds clearly shows the monotonous variation of the rebound speed with the incident speed. The second plot in Fig. 8 shows that the rebound angle plots are identical for different ball speeds. The plot suggests that the rebound angle is influenced only by the incident angle for a rolling ball with no sidespin prior to the impact.

Figure 9 depicts the rebound conditions for a ball incident speed of 1 m/s with different types of spin colliding with the cushion at different incident angles. According to Fig. 9, when the ball is overspinning before the collision, its rebound tends to be generally higher. When the topspin of the ball is $\omega_0^{\mathrm{T}} = 2V_0/R$, at a 90° incident angle, the rebound speed reaches the incident speed value of V_0. For any given speed–spin conditions, the speed loss is largest for the ball incident angles around 40°. The rebound angles are not greatly affected by the excessive topspin of the ball as seen in the second plot of Fig. 9.

Figure 10 shows the rebound characteristics for a rolling ball with different sidespin values. The plots provide some very interesting results. Also, when the ball has right spin (according to billiards terminology, the direction of ω_0^S – as marked in Fig. 2 – is called right spin, the opposite of which is left spin), the rebound speed exceeds the value of the incident speed. In addition, for higher values of left spin, at higher incident angles towards 90°, the rebound velocity exceeds the value of the incident ball speed. The second plot in Fig. 10 suggest that when the ball has left spin ($k < 0$), and for incident angle values close to 90°, the ball bounces back to the side from which it approached the cushion (see Fig. 11). This effect of the ball rebounding to the same side has been described by Walker [**17**] for billiards, and by Cross [**18**] in a general context for the bounce of a ball. Cross [**18**] also provides the experimental results for the rebound characteristics of a tennis ball bouncing on a rough surface.

A plot of sliding speeds against the instantaneous impulse value is shown in Fig. 12. The change in slip directions as indicated by the plot suggests that the assumption of unidirectional slip cannot be true.

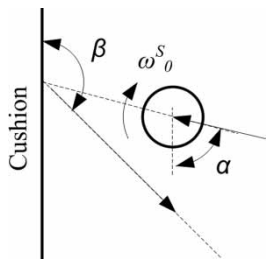

Fig. 11 Ball bouncing back to the same side under left spin conditions for α's close to 90°

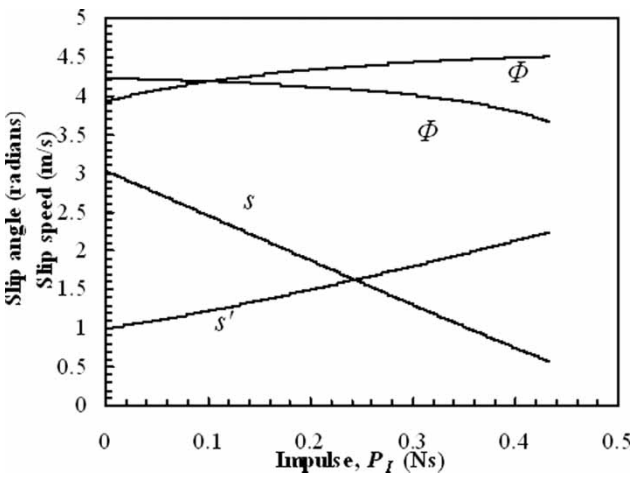

Fig. 12 Slip–impulse curves for $V_0 = 2\,\text{m/s}$, $\alpha = 45°$, $\omega_0^S = 2V_0/R$, and $\omega_0^T = 1.5V_0/R$ (s and Φ are for the slip at the cushion, and s' and Φ' are for the slip at the table)

5 CONCLUSIONS

A 3D impact analysis for the collision of a spinning billiard ball with a cushion is presented. Differential equations are derived for ball dynamics during the time of impact and then the solutions are found numerically.

Combining some of the authors' previous experimental results with the numerical solutions, the coefficient of restitution for the ball–cushion collision is determined as 0.98. In addition, the value for the sliding coefficient of friction is found to be 0.14.

The rebound angles and speeds are given as plots against the incident angles and speeds for different velocities and spin conditions. Under excessive sidespin conditions, the rebound speeds are found to exceed the incident speeds and the ball is also found to bounce back on the side from which it approached the cushion.

Although this analysis provides the quantification for many phenomena involved with cushion collisions that are described in the billiards literature, it is expected to be validated by tracking the spin of a billiard ball. A colour pattern drawn on a white cue ball may be used for this purpose.

REFERENCES

1 **Nadler, D.** *Mathematical theory of spin, friction, and collision in the game of billiards*, 2005. An English translation of Coriolis' 1835 book (Nadler, D., San Francisco, California, USA).

2 **Long, F., Herland, J., Tessier, M.-C., Naulls, D., Roth, A., Roth, G.,** and **Greenspan, M.** Robotic pool: an experiment in automatic potting. In Proceedings of the IROS'04: IEEE/RSJ International Conference on *Intelligent and robotics and systems*, Sendai, Japan, 2004, vol. 3, pp. 2520–2525.

3 **Ho, K. H. L., Martin, T.,** and **Baldwin, J.** Snooker robot player – 20 years on. In Proceedings of the IEEE Symposium on *Computational intelligence and games* (CIG 2007), Hawaii, 1–5 April 2007, pp. 1–8.

4 **Cheng, B.-R., Li, J.-T.,** and **Yang, J.-S.** Design of the neural-fuzzy compensator for a billiard robot. In Proceedings of the 2004 IEEE International Conference on *Networking, sensing and control*, Taipei, Taiwan, 21–23 March 2004, pp. 909–913.

5 **Alian, M. E., Shouraki, S. E., Shalmani, M. T. M., Karimian, P.,** and **Sabzmeydani, P.** Roboshark: a gantry pool player. In Proceedings of the 35th International Symposium on *Robotics* (ISR), Paris, France, 2004.

6 **Jebara, T., Eyster, C., Weaver, J., Starner, T.,** and **Pentland, A.** Stochasticks: augmenting the billiards experience with probabilistic vision and wearable computer. In Proceedings of the IEEE International Symposium on *Wearable computers*, Cambridge, MA, USA, October 1997, pp. 138–145.

7 **Larsen, L. B., Jensen, M. D.,** and **Vodzi, W. K.** Multi modal user interaction in an automatic pool trainer. In Proceedings of the Fourth IEEE International Conference on *Multimodal interfaces* (ICMI'02), Pittsburgh, USA, 14–16 October 2002, pp. 361–366.

8 **Uchiyama, H.** and **Saito, H.** AR display of visual aids for supporting pool games by online markerless tracking. In Proceedings of the 17th International Conference on *Artificial reality and telexistence* (ICAT 2007), Esbjerg, Denmark, 28–30 November 2007, pp. 172–179.

9 **Smith, M.** PickPocket: a computer billiards shark. *Artif. Intell.*, 2007, **171**(16–17), 1069–1091.

10 **Dussault, J.-P.** and **Landry, J.-F.** Optimization of a billiard player – tactical play. *Lect. Notes Comput. Sci.*, 2007, **4630**, 256–270.

11 **Leckie, W.** and **Greenspan, M.** An event-based pool physics simulator. *Lect. Notes Comput. Sci.*, 2006, **4250**, 247–262.

12 **Marlow, W. C.** *The physics of pocket billiards*, 1994 (MAST, Florida, USA).

13 **Alciatore, D. G.** Pool and billiards physics principles by coriolis and others. *Am. J. Phys.* (submitted), available from http://billiards.colostate.edu/physics/Alciatore_AJP_MS22090_revised_pool_physics_article.pdf. (access date 20 January 2009).

14 **de la Torre Juárez, M.** The effect of impulsive forces on a system with friction: the example of the billiard game. *Eur. J. Phys.*, 1994, **15**(4), 184–190.

15 **Stronge, W. J.** *Impact mechanics*, 2000 (Cambridge University Press, Cambridge, UK).

16 **Mathavan, S., Jackson, M. R.,** and **Parkin, R. M.** Application of high-speed imaging in determining the dynamics involved in billiards. *Am. J. Phys.*, 2009, **77**(9), 788–794.

17 **Walker, J.** The physics of the follow, the draw and the masse (in billiards and pool). *Sci. Am.*, 1983, **249**, 124–129.

18 **Cross, R.** Bounce of a spinning ball near normal incidence. *Am. J. Phys.*, 2005, **73**(10), 914–992.

APPENDIX

Notation

e_e	coefficient of restitution between the ball and the cushion
F	force
I	moment of inertia of the ball
M	mass of the ball
N	number of iterations
P	accumulated impulse at any time during impact
P_I^c	accumulated impulse at the termination of compression
P_I^f	the final accumulated value of impulse
R	radius of the ball
s	slip speed
V_0	incident speed of the ball
W	work done due to impulse force
α	ball incident angle with the cushion
β	rebound angle
ΔP	impulse during a time of Δt
θ	the angle that the common normal of the ball–cushion contact point makes with the horizontal
$\dot{\theta}$	angular velocity of the ball
μ_s	coefficient of sliding friction between the ball and the table
μ_w	coefficient of sliding friction between the ball and the cushion
Φ	direction of slip
ω_0^S	sidespin of the ball at incidence
ω_0^T	topspin of the ball at incidence